Elastic recoil detection studies of near-surface hydrogen in cavity-grade niobium

2011 Supercond. Sci. Technol. 24 105017

(http://iopscience.iop.org/0953-2048/24/10/105017)

Supercond. Sci. Technol. **24** (2011) 105017 (5pp) doi:10.1088/0953-2048/24/10/105017

Elastic recoil detection studies of near-surface hydrogen in cavity-grade niobium

A Romanenko[1] **and L V Goncharova**[2]

[1] Fermi National Accelerator Laboratory, Batavia, IL 60510, USA
[2] Department of Physics and Astronomy, University of Western Ontario, London, ON N6A 3K7, Canada

E-mail: aroman@fnal.gov

Received 19 July 2011, in final form 17 August 2011
Published 13 September 2011
Online at stacks.iop.org/SUST/24/105017

Abstract
Recent studies of the quality factor degradation mechanisms in superconducting RF niobium cavities at high surface magnetic fields revealed that RF performance may depend on the total hydrogen content in the 40 nm thick near-surface layer. Hydrogen distribution in niobium and its near-surface content variations after different chemical surface treatments has been addressed in previous studies. However, only chemical treatments were studied while heat treatments are equally important. In this work we use the elastic recoil detection (ERD) technique to systematically study the distribution of hydrogen in niobium sheet and cavity cutout samples subjected to chemical and heat treatments typically performed on niobium cavities. Our results indicate the near-surface segregation of hydrogen at the niobium oxide/niobium interface, and do not show any significant variation in hydrogen content after various heat and chemical treatments. We do not observe a direct correlation between total hydrogen content and the high field Q slope. Consequences of the observed hydrogen segregation are discussed in the framework of the NbH_x phase diagram.

(Some figures in this article are in colour only in the electronic version)

1. Introduction

Superconducting RF (SRF) cavities made of bulk niobium are used as primary accelerating components in a number of present and future accelerators based on the superconducting technology. Significant progress has been made in the last few years in achieving larger accelerating gradients in SRF cavities. Nevertheless, full understanding of the surface structure of niobium used in cavities is not yet developed. One area of recent active research is the contributions of different near-surface lattice defects to the cavity performance at high fields, and in particular on a high field Q slope (HFQS) (see [1] for a review). An underlying mechanism of a strong effect of the *in situ* vacuum baking at 120 °C for 48 h on the high field performance of niobium cavities remains controversial.

A key question is what particular material intrinsic or extrinsic properties are leading to the RF losses in the HFQS. A closely related and equally important question is what changes in the niobium near-surface composition and structure at 120 °C. Several niobium defects, such as dislocations [2], vacancies [3] and near-surface interstitial hydrogen [4] are currently considered as possible causes of the HFQS and all can be active in the experimentally observed mild baking effect. For all three types of defects, it is crucial to understand their distribution and change on the scale of magnetic field penetration depth (about 40 nm) during cavity processing treatments. In particular, for dislocations and vacancies, hydrogen may be involved in the mild baking effect via vacancy–hydrogen complexes [5], while the interstitial hydrogen model relies on the changes of hydrogen content itself during different treatments. An earlier study [6] explored the effect of different chemical etching solutions on the near-surface hydrogen content with the depth resolution limited at the time to about 30 nm due to the detection method. In this study we advance the hydrogen distribution issue by using ERD on samples treated using different thermal and chemical etching steps with known outcomes on RF cavities. Additionally ERD spectra of two cavity cutout samples were

Table 1. Hydrogen profiling results. Quantitative fittings of hydrogen distribution are obtained based on the niobium surface layer model from figure 3, with x, y, b corresponding to the fraction of hydrogen in, respectively, oxide, near-surface layer and bulk niobium.

Sample	Treatment	Enriched layer (nm)	x	y	b
HA-1	BCP 150 μm	4	0.15	0.15	0.008
HA-2	BCP 150 μm + 800 °C 4 h	3.6	0.11	0.11	0.006
HA-3	BCP 150 μm + 800 °C 4 h + 110 °C 74 h	2.7	0.15	0.15	0.008
HA-4	BCP 150 μm + 800 °C 4 h + 110 °C 74 h + HF rinsing 20 min	8/25	0.09	0.09/0.04	0.008
HA-5	BCP 150 μm + 600 °C 10 h	4	0.19	0.19	0.006
HA-6	BCP 150 μm + 600 °C 10 h +110 °C 54 h	4	0.11	0.11	0.006
LE1-37 hot spot	BCP 200 μm	0.7	0.16	0.16	0.006
TE1AES004 cold spot	EP 120 μm + 120 °C 48 h	0.7	0.16	0.16	0.006

measured and correlated with their drastically different RF behavior.

2. Experimental details

2.1. Sample preparation and RF tests

Two types of samples have been used in this study:

(i) Rectangular 1.2 cm × 1.5 cm, 3 mm thick samples cut with the wire electrical discharge machining (EDM) from the RRR 300 single-grain niobium sheet and subjected to 150 μm buffered chemical polishing after cutting. Six different treatment sequences have been used and the corresponding samples are named HA-1 to HA-6: HA-1—BCP only; HA-2—additional 800 °C 4 h vacuum bake; HA-3—same as HA-2 with additional 110 °C vacuum bake for 74 h; HA-4—same as HA-3 with an additional hydrofluoric acid (HF) rinse for 20 min; HA-5—BCP and 600 °C vacuum baking for 10 h; HA-6—same as HA-5 with additional 110 °C bake for 54 h in vacuum.

(ii) Circular cutouts from: (i) a large grain (∼10 cm) buffered chemical polished (BCP) cavity (LE1-37) limited by the HFQS; (ii) a fine grain (∼50 μm) electropolished (EP) cavity (TE1AES004) free of the HFQS.

Niobium sheet samples were subjected to a sequence of surface treatments similar to those performed on cavities with known outcomes on RF performance. Several different surface treatments were tried including (i) vacuum baking at 600 °C for 10 h, (ii) 800 °C for 4 h, (iii) 120 °C for 48 h and (iv) rinsing in concentrated (48%) hydrofluoric acid (HF) for 20 min. Details of the treatments with the list of samples used in the studies are shown in table 1. Cavity cutout samples come from two different cavities: large-grain BCP cavity LE1-37, with a grain size of about 10 cm, and a fine-grain TE1AES004 EP cavity, with a grain size of about 50 μm. TE1AES004 was subjected to 120 °C 48 h vacuum treatment to eliminate the HFQS. The LE1-37 cavity was limited by the HFQS and the cutout represents an area with high RF losses in the HFQS regime (hot spot). Details on LE1-37 cavity tests and surface analytical techniques applied on cutouts are reported elsewhere [5, 7, 8]. The TE1AES004 cutout represents an area without any RF losses (cold spot) up to the highest field reached, which was determined by the localized quench at a different location. Full analysis of other TE1AES004 cutouts using alternative techniques is currently underway and will be published elsewhere. Temperature increase of the outside cavity wall was registered with carbon resistance thermometers during the RF test for both cutouts at each field level and the results are shown in figure 1.

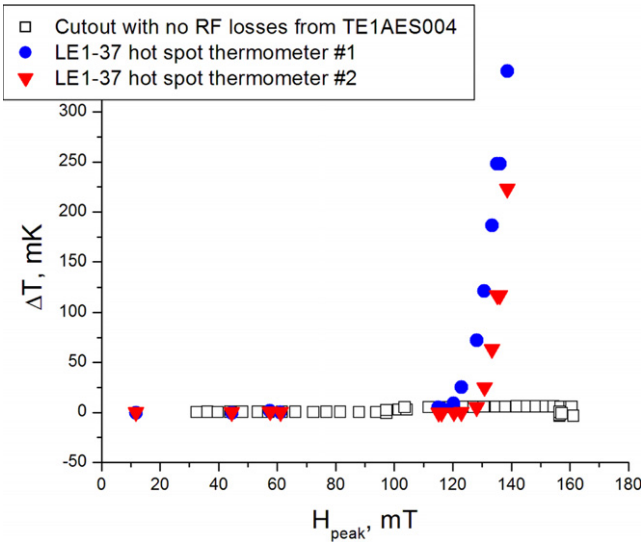

Figure 1. Temperature variations of the outside cavity walls in the cutout regions during RF tests at different magnetic field levels. LE1-37 cutout had two thermometers attached during the RF test separated by about 1 cm, and both registered a strong HFQS heating starting from about 120 mT (solid red triangles and blue circles). TE1AES004 cutout (empty squares) exhibited no temperature increase up to the highest field.

2.2. Hydrogen ERD analysis

Niobium samples were studied using a 1.6 MeV ^{4}He beam in a conventional ERD set-up with incident angle of 75°, recoil angle of 30° and 6.1 μm Al-coated mylar range foil. IBM geometry was used where incident beam, exit beam and the surface normal are in the same plane [9]. Kapton and H-implanted Si targets were used as standards to determine the detector solid angle, both agreed at ∼3%. Charge collection was monitored by an intermittent Faraday cup that intercepts the beam in front of the target with a duty cycle (beam-on-target fraction) of ∼75%. An HF-etched Si sample exposed to air for a short period of time was analyzed to estimate possible surface hydrocarbon contamination. Note that all ERDA data represent averages over a sample area (2–10 mm^2); this makes it difficult for us to distinguish between hydrogen

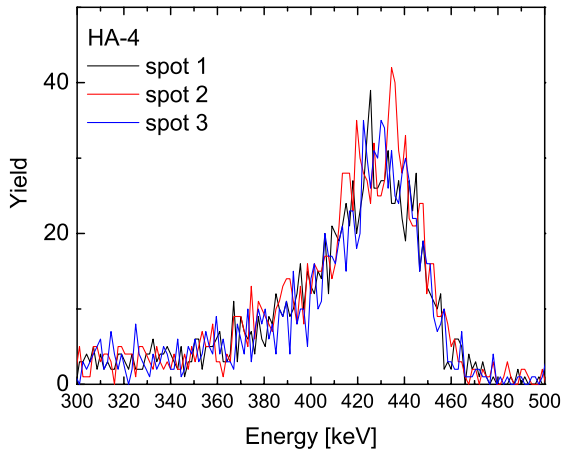

Figure 2. Spot-to-spot variation of elastic recoil yield (in arbitrary units) for HA-4 sample. Other samples exhibited similar low variation.

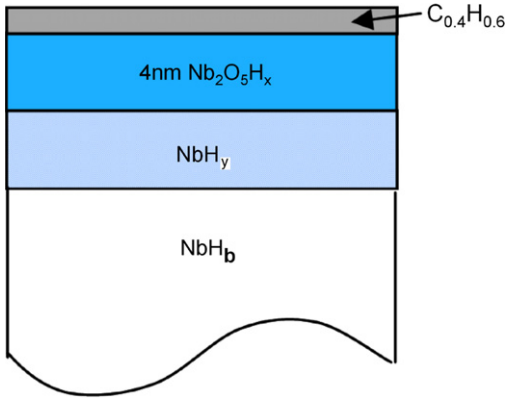

Figure 3. Surface structure of Nb assumed for ERD data fitting.

compositional gradient and roughness at the NbH_y/NbH_b interface [10, 11].

Measurements were performed at multiple spots on each sample separated by at least 1–2 mm, and a typical spot-to-spot variation is shown in figure 2 on the example of sample HA-4. The spot-to-spot variation is below 5% (as calculated from integrated near-surface intensity for the 375–480 keV energy window), suggesting a uniform distribution of hydrogen over the sample surface. Similar results were obtained on all other investigated samples.

SIMNRA, v. 6.05 [9] was used to fit experimental data in order to extract the depth profiles of hydrogen concentration. We assume the surface composition of bulk niobium as shown in figure 3, which is a generally accepted structure deduced by surface analytical techniques such as TEM, XPS, AES and SIMS.

Several assumptions were made for fitting the data in order to obtain the depth distribution of hydrogen. In particular, total hydrogen yield in experimental ERDA spectra was reduced by an H atomic density of 6×10^{15} at. cm^{-2}. This amount is roughly equivalent to the 10–12 Å thick layer of hydrocarbons ($C_{0.4}H_{0.6}$) or alternatively hydrogen-containing molecules giving rise to additional hydrogen yield from the surface. Calculated hydrogen peak intensity corresponding to this hydrogen atomic density was subtracted from the experimental intensity for samples HA1–6.

The surface layer of 4 nm thick Nb_2O_5 (density = 4.47 g cm^{-3}) was assumed. Bulk Nb density (8.7 g cm^{-3}) was used for the deepest NbH_b layer and an interfacial NbH_x layer density of 7.72 g cm^{-3} was applied for thickness calculations (assuming roughly 10% hydrogen content).

2.3. Results on Nb sheet samples

The summary of the ERDA results for niobium sheet samples is presented in figure 4. Note that the spectra for only four samples are shown for clarity. The observed hydrogen distributions reveal the near-surface segregation in all samples within the first few nanometers while the bulk hydrogen content is below 1 at.% and does not vary dramatically between the samples. Note that the ERDA detection limit is of the order of 20 at. ppm. The hydrogen-enriched layer is about 8–9 nm thick for all samples (except HA-4), which includes 4 nm of Nb_2O_5 used for the best fit as described above. Comparison of hydrogen profiles (figure 4) for samples HA-1, HA-2 and HA-3 indicates that hydrogen content is reduced after consecutive heat and chemical treatments. Hydrogen depth distribution is significantly different for the HA-4 sample, which was rinsed in HF for 20 min following the 800 °C 4 h and 110 °C 74 h high temperature treatments. In the HA-4 sample hydrogen enrichment is extended to about 40 nm deep with the hydrogen gradient slowly decreasing into the Nb bulk (as shown schematically by two layers of different hydrogen content in the right panel of figure 4). Note that hydrogen concentration in the near-surface region is lower in sample HA-4 compared to other samples.

2.4. Results on cavity cutouts

If the near-surface hydrogen is the primary cause of the observed difference in RF behavior of the cavity cutouts (figure 1), we would expect to observe a difference in hydrogen depth profiles. However, we observe exactly the same hydrogen distributions in both cavity cutouts as shown in figure 5, along with the typical spot-to-spot variation shown for the TE1AES004 cutout.

ERDA results and calculated depth profiles show hydrogen enrichment for cavity cutouts, but the depth of the enriched layer is shorter than in the niobium sheet samples. The concentration of hydrogen at the niobium oxide/niobium interface is about 16 at.%, which is comparable to the niobium sheet samples.

3. Discussion

One of the possible causes for the HFQS and its sensitivity to different treatments may be due to differences in near-surface hydrogen content. There is some correlation reported between the cavity performance and the concentration of hydrogen from secondary ion mass spectrometry (SIMS) measurements on control samples treated with the cavity [4]. But the quantification of profiles in SIMS is a challenge due to the matrix effects and uncertainty of ionization yields at

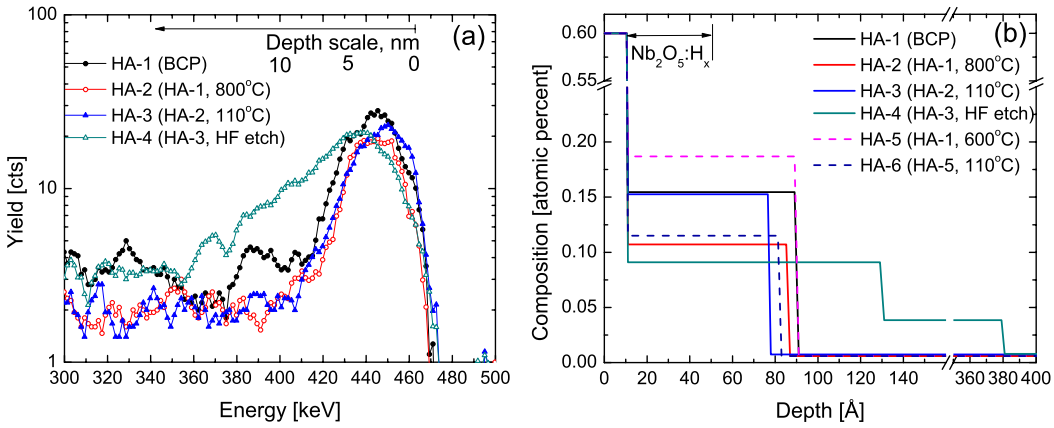

Figure 4. Experimental data (a) and the depth profile of hydrogen atomic per cent obtained by fitting the data (b). An uncertainty in the calculated hydrogen percentage is estimated to be about 5%.

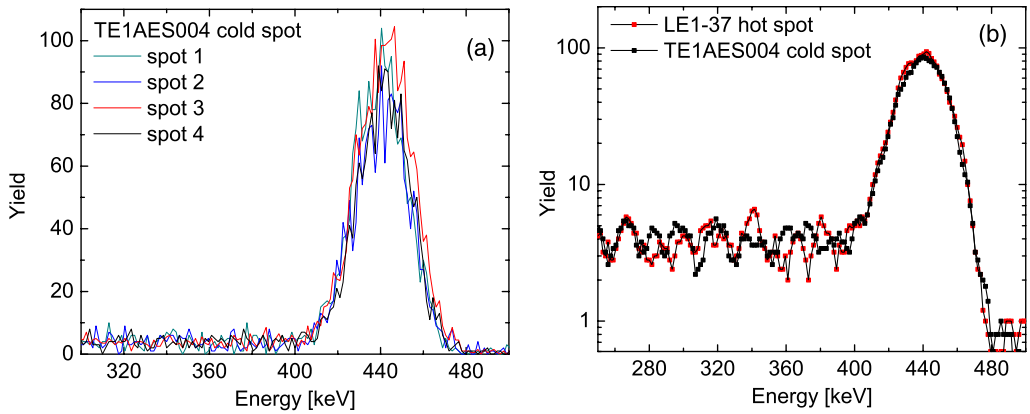

Figure 5. Spot-to-spot variation of the recoiled ion yield (in arbitrary units) (a) and raw data on LE1-37 and TE1AES004 cavity cutouts (b). Both spectra are strikingly similar even though they come from completely different cavities exhibiting drastically different RF losses with field.

the interfaces. Our results do not support the correlation between the concentration of hydrogen in the near-surface layer and cavity performance. The most significant result is almost exactly the same hydrogen depth profile in cutout samples coming from the large-grain BCP cavity hot spot and a fine-grain EP cavity cold spot. (Local heating registered at these locations during respective cavity tests is drastically different—a strong HFQS heating up to a few hundred mK in one case starting from about 100 mT, and no registered heating at all in the other case up to 160 mT.) This result strongly suggests that there is no direct role of interstitial hydrogen in the HFQS. But, since ERD does not distinguish between hydrogen in the interstitials and precipitates, it may be possible that the difference in losses comes from different precipitation states in these two samples rather than different amounts of hydrogen dissolved in the lattice. Furthermore, hydrogen can still be involved indirectly in the mild baking effect via dissociation of vacancy–hydrogen complexes resulting in the free vacancy mobility.

Another result is a significant near-surface hydrogen segregation in all samples. The absolute atomic concentration of H in the Nb lattice is very high and ranges from 9 to 19 at.%. Such a high hydrogen content should lead to the abundance of hydrogen-induced lattice defects such as vacancy–hydrogen complexes [12]. If the ordered hydride phases are precipitated, misfit dislocations are also possible [13], which may account for possible differences between surface and bulk dislocation densities. In addition, this level of hydrogen corresponds to the mixed $\alpha + \beta$ phase at room temperature in the phase diagram from [14]. This finding indicates that precipitates of the β phase may be present in the surface layer of all niobium cavities independent of the standard heat treatments chosen if nucleation sites exist for precipitates to form. The recent discovery of dendritic hydrides in lossy areas of cavity walls at high magnetic fields [15] confirms this conclusion.

Systematic studies following the cavity surface treatment path show that H concentration in the first few nanometers does not change significantly during heat treatments and does change after HF rinsing, resulting in the hydrogen-rich layer extending to a greater depth. We speculate that this effect might be caused by the removal of the natural oxide layer during HF rinsing, which normally serves as a barrier for additional hydrogen adsorption. The removal of the so-called hydrogen Q disease by 600–800 °C annealing observed in SRF niobium cavities is thus not necessarily caused by the change in the near-surface hydrogen content. An alternative mechanism should be present, which prevents the formation of hydride phases during slow cooling-down steps.

Finally we note that niobium sheet samples used for the studies did not go through severe mechanical deformation as in the case of cavity deep drawing used to form half-cells from niobium sheets. In principle, the mobility of hydrogen during heat treatments should be affected by the presence of dislocations and vacancies, which serve as hydrogen trapping sites. Hence we intend in future work to perform similar studies along the cavity processing steps with samples pre-deformed to a different degree and cavity cutouts subjected to further heat and chemical treatments.

4. Conclusion

Using elastic recoil detection technique on niobium sheet samples subjected to different treatments along SRF cavity processing steps, we demonstrate a near-surface hydrogen enrichment, which is not removed by 800, 600 and 120 °C heat treatments typically applied to cavities. The level of hydrogen in the near-surface region indicates the possible room temperature presence of both α and β phases as well as the possibility of hydrogen-induced lattice defects such as vacancies and dislocations. Comparison between cavity cutouts exhibiting drastically different RF behaviors shows the same hydrogen depth profile, contradicting the hypothesis of the difference in hydrogen content as a reason behind the high field Q slope of superconducting niobium cavities. Different amounts of precipitation for the same total amount of hydrogen may be the real reason behind the difference in RF losses.

Acknowledgments

We would like to acknowledge valuable discussions with L Cooley and G Wu from Fermilab, A Grassellino from TRIUMF and H Padamsee from Cornell University. We thank G Ciovati from Jefferson Lab for the TE1AES004 cavity test with thermometry and J Hendriks of the Western Tandetron Accelerator Facility for valuable help with the ion beam analysis.

References

[1] Padamsee H 2009 *RF Superconductivity* vol II *Science, Technology and Applications* (Weinheim: Wiley–VCH)
[2] Romanenko A and Padamsee H 2010 *Supercond. Sci. Technol.* **23** 045008
[3] Visentin B, Barthe M F, Moineau V and Desgardin P 2010 *Phys. Rev. Spec. Top. Accel. Beams* **13** 052002
[4] Ciovati G, Myneni G, Stevie F, Maheshwari P and Griffis D 2010 *Phys. Rev. Spec. Top. Accel. Beams* **13** 022002
[5] Romanenko A 2009 Surface characterization of niobium cavity sections: understanding the high field Q-slope *PhD Thesis* Cornell University
[6] Antoine C Z *et al* 1991 The role of atomic hydrogen in Q-degradation of niobium superconducting rf cavities: analytical point of view *Proc. 5th Workshop on RF Superconductivity (DESY, Hamburg)* pp 616–34
[7] Romanenko A, Padamsee H, Eremeev G and Shu J 2007 Comparative surface studies on fine-grain and single crystal niobium using XPS, AES, EBSD and profilometry *Proc. PAC2007*
[8] Romanenko A 2009 Crystalline microstructure role in the high-field Q-slope *Proc. 14th Int. Conf. on RF Superconductivity*
[9] Mayer M 1997 *SIMNRA User's Guide IPP* 9/113 Max-Planck-Institut fur Plasmaphysik, Garching, Germany
[10] Molodtsov S L, Gurbich A F and Jeynes C 2008 *J. Phys. D: Appl. Phys.* **41** 205303
[11] Schulte W H, Busch B W, Garfunkel E, Gustaffson T, Schiwietz G and Grande P L 2001 *Nucl. Instrum. Methods* B **183** 16–24
[12] Cizek J, Prochazka I, Kuzel R, Becvar F, Cieslar M, Brauer G, Anwand W, Kirchheim R and Pundt A 2005 *J. Alloys Compounds* **404–406** 580–3
[13] Makenas B and Birnbaum H 1980 *Acta Metall.* **28** 979–88
[14] Manchester F D and Pitre J M 2000 *Phase Diagrams of Binary Hydrogen Alloys* (Materials Park, OH: ASM International)
[15] Romanenko A, Wu G, Ciovati G and Cooley L D 2011 Post-baking losses in electropolished niobium cavities: dissection studies *Proc. 15th Int. Conf. on RF Superconductivity* p ThPO08